Histol Histopathol (2025) 40: 697-710

Histology and Histopathology
From Cell Biology to Tissue Engineering

ORIGINAL ARTICLE Open Access

Tetrahydropalmatine promotes macrophage autophagy by inhibiting the AMPK/mTOR pathway to attenuate atherosclerosis

Hui Wang[1], Ke Ding[2], Jiaqi He[3] and Jiahong Wang[3]

[1]Zhejiang Chinese Medical University, [2]Department of Pharmacy, The First Affiliated Hospital of Zhejiang Chinese Medical University and [3]Traditional Chinese Medicine Dispensary, The First Affiliated Hospital of Zhejiang Chinese Medical University, Hangzhou, Zhejiang, China

Summary. Background. Atherosclerosis (AS) is a chronic progressive arterial disease that is associated with macrophage autophagy and AMP-activated protein kinase (AMPK)/mechanistic target of the rapamycin (mTOR) pathway. Tetrahydropalmatine (THP) can activate AMPK-dependent autophagy. We aim to study the mechanism of macrophage autophagy mediated by THP in the treatment of AS via the AMPK/mTOR pathway.

Methods. High-fat diet apolipoprotein E-deficient mice and ox-LDL-induced RAW264.7 cells were used to mimic the AS model, then THP was administered. Cell viability was detected by MTT. Pathological aorta lesions were detected using Hematoxylin and Eosin, Masson, and oil red staining. Lipid metabolism indices and inflammatory factors were measured using ELISA. A transmission electron microscope was used to observe autophagosomes. Autophagy and AMPK/mTOR pathway protein expression was detected by immunofluorescence and Western blot. The AMPK inhibitor 9-β-d-Arabinofuranosyl Adenine (Ara-A) was used to validate the effect of THP. The mRNA expression of *Beclin-1* and *MCP-1* was detected by q-PCR.

Results. THP administration regulated lipid metabolism by lowering total cholesterol, triacylglycerol, low-density lipoprotein, and high-density lipoprotein levels, and suppressed aortic damage. THP suppressed aortic damage and regulated lipid metabolism by altering serum lipid levels. THP reduced inflammation and macrophage CD68 expression. Twenty μg/mL THP reduced cell viability. THP decreased cholesterol uptake and increased efflux, promoting autophagy. THP increased autophagosome number, LC3B expression, and autophagy markers p-AMPK/AMPK and LC3-II/LC3-I. THP also decreased p-mTOR/mTOR and P62. THP increased *Beclin-1* mRNA expression and decreased *MCP-1* mRNA expression. Ara-A reversed THP's effects.

Conclusion. THP promotes macrophage autophagy by inhibiting the AMPK/mTOR pathway to attenuate AS.

Key words: Atherosclerosis, Tetrahydropalmatine, Macrophage autophagy, Lipid metabolism, AMPK/mTOR pathway

Introduction

Atherosclerosis (AS) is a common disease with high morbidity and 230 million people have been affected worldwide (Song et al., 2020). Cardiovascular and cerebrovascular diseases based on AS have an extremely high probability of disability and death, thus seriously threatening human health (Tabares-Guevara et al., 2021). The American Heart Association estimates that, worldwide, cardiovascular disease kills approximately tens of millions of people each year (Mozaffarian et al., 2015). The pathogenesis of AS involves a variety of pathological processes (Osonoi et al., 2018), mainly including endothelial cell dysfunction, abnormal

Corresponding Author: Ke Ding, Department of Pharmacy, The First Affiliated Hospital of Zhejiang Chinese Medical University, No. 54, Youdian Road, Hangzhou, Zhejiang, China. e-mail: ko_ding@hotmail.com

www.hh.um.es. DOI: 10.14670/HH-18-809

Abbreviations. AS, Atherosclerosis; AMPK, AMP-activated protein kinase; mTOR, mechanistic target of rapamycin; THP, Tetrahydropalmatine; Ara-A, 9-β-d-Arabinofuranosyl Adenine; ApoE-/-, apolipoprotein E deficient; ox-LDL, Oxidized-low density lipoprotein; TC, Total cholesterol; TG, triacylglycerol; LDL, low-density lipoprotein; HDL, high-density lipoprotein; MCP-1, monocyte chemoattractant protein-1; TNF-α, tumor necrosis factor-α; IL-6, interleukin-6; HE, Hematoxylin and Eosin; IF, Immunofluorescence; TEM, Transmission electron microscope; ANOVA, analysis of variance; SD, standard deviation.

proliferation of vascular smooth muscle cells, and foam cell formation (Yuan et al., 2012; Chistiakov et al., 2017). Among them, the aggregation of macrophages in the intima plays a crucial role in the formation and stabilization of early AS plaques (Evans et al., 2018; Yang et al., 2018). In addition, excessive lipid uptake causes macrophages to form foam cells, which leads to the development of AS (Wang et al., 2022). Studies have shown that the autophagy process of macrophages is significantly damaged after lipid load stimulation (Sergin and Razani, 2014). impaired autophagy of macrophages leads to excessive activation of the inflammasome, which further promotes the progression of AS by enhancing the production of inflammatory cytokines (Razani et al., 2012). In addition, inhibition of autophagy promotes the transformation of foam cells and the development of plaques (Emanuel et al., 2014). Therefore, it is of great significance to investigate the role of autophagy in lipid-stimulated macrophages.

The AMP-activated protein kinase (AMPK)/ mechanistic target of the rapamycin (mTOR) pathway is a significant signaling pathway in the formation of AS (Sundararajan et al., 2019). Studies have shown that the AMPK/mTOR pathway mediates macrophage autophagy and inflammation (Fan et al., 2015), and inhibits the formation of AS plaques (Cao et al., 2020). In addition, Takeda-Watanabe et al. confirmed that Sirtinol, a SIRT1 inhibitor, increases the expression of pro-inflammatory genes in macrophages, induces autophagy defects, and decreases AMPK activity, while the mTOR inhibitor rapamycin eliminates the adverse effects of Sirtinol (Takeda-Watanabe et al., 2012). These results suggest that intervening in the AMPK/mTOR pathway to promote macrophage autophagy could be an effective treatment for AS.

At present, it is of great significance to search for drugs that have little toxicity and side effects and can effectively intervene, or even reverse, AS. Tetrahydropalmatine (THP) is the main component of *Corydalis yanhusuo* W. T. Wang, and it has been found to participate in the regulation of various diseases through the activation of AMPK-dependent autophagy (Cao et al., 2019; Yin et al., 2022b). Yin et al. found that THP inhibits the growth of hepatocellular carcinoma in nude mice by promoting autophagy (Yin et al., 2021). In addition, THP can induce M1 macrophages to convert to M2 to inhibit inflammation, which is related to the enhancement of autophagy (Wen et al., 2022). So, we speculate that THP could regulate the AMPK/mTOR pathway to activate macrophage autophagy and alleviate AS. 9-β-d-Arabinofuranosyl Adenine (Ara-A), an AMPK inhibitor (Guan et al., 2008), is used to study the effects of THP on macrophage autophagy via AMPK/mTOR pathway.

In this study, apolipoprotein E-deficient ($ApoE^{-/-}$) mice were fed a high-fat diet to establish a classical AS animal model (Bai et al., 2020) and explore the effect of THP on improving AS. Oxidized-low density lipoprotein (ox-LDL) was applied to stimulate AS in RAW264.7 cells and the mechanism of macrophage autophagy in alleviating AS by THP was studied. This systematic study on the anti-AS effects and mechanism of THP is expected to provide a new theory and new ideas for the clinical intervention of THP in the prevention and treatment of AS.

Materials and methods

Reagents and chemicals

Tetrahydropalmatine (THP, Y39962), oxidized-low density lipoprotein (ox-LDL, S24879), and Ara-A (B25665) were obtained from Shanghai Yuanye Bio-Technology Co., Ltd (China). The kits for total cholesterol (RXWB0011-96), triacylglycerol (TG) (RXWB0294-96), mouse low-density lipoprotein (LDL, RX202979M), mouse high-density lipoprotein (HDL, RX202924M), mouse monocyte chemoattractant protein-1 (MCP-1) ELISA, mouse tumor necrosis factor-α (TNF-α) ELISA (RX202412M), and mouse interleukin-6 (IL-6) ELISA (RX203049M) were purchased from Quanzhou Ruixin Biotechnology Co., Ltd (China). The Cholesterol Uptake Assay kit (ab236212) and Cholesterol Efflux Assay (ab196985) kit were provided by Abcam (USA). LC3B (AF4650), CD68 (DF7518), AMPK (Ab133448), p-AMPK (AF3423), mTOR (AF6308), p-mTOR (AF3308), P62 (AF5384), LC3 (AF5402) antibodies were provided by Affinity (USA). The GAPDH antibody (10494-1-AP) was purchased from Proteintech (USA).

Ethics

The experimental animals were reviewed by the Experimental Animal Ethics Committee of Zhejiang Eyoung Pharmaceutical Research and Development Co., Ltd (License No.: SYXK (Zhe) 2021-0033).

Animals

Male C57BL/6J mice (16-18 g weight, 6 weeks old) and male $ApoE^{-/-}$ mice (C57BL/6J background, 16-18 g weight, 6 weeks old) were provided by Hangzhou Qizhen experimental animal technology Co., LTD of animal license permit number: SCXK (Zhe) 2022-0005. Animals were transferred to the SPF animal room of Zhejiang Eyoung Pharmaceutical Research and Development Co., Ltd for one week of adaptive feeding. The animal room conditions were 12h dark/light cycles at 23±2°C and humidity of 60±5%.

Animal model and administration

Six C57BL/6J mice served as the Control group. Eighteen $ApoE^{-/-}$ mice were randomly divided into three groups: the AS and THP groups (10 mg/kg and 40 mg/kg (Mao et al., 2015)). To establish an animal model of AS, mice of the AS group and the THP groups were

raised on a purified high-fat diet (0.15% cholesterol and 21% fat (Liang et al., 2020)) while the Control group was fed with a normal chow. Mice of the THP groups were given 10 mg/kg and 40 mg/kg THP while the Control and the AS group were administered equal amounts of normal saline for 8 weeks.

After the last administration, blood was extracted from the eyeball after inhalation anesthesia with isoflurane and then centrifuged (4°C, 3500 r/min, 10 min) for 1h to obtain the serum. The mice were euthanized with CO_2, the aorta tissues were quickly separated and fixed in 4% paraformaldehyde or stored at -80°C for subsequent experiments.

Hematoxylin and Eosin (HE) staining

The aorta tissues were separated, fixed in 4% paraformaldehyde, and embedded in paraffin wax, followed by cutting into 5-μm slides. The xylene and gradient ethanol were used to de-wax the slides, followed by washing with water and staining with hematoxylin and eosin. The slides were dehydrated using gradient ethanol and sealed with neutral gum. The image acquisition and analysis of the slides at 200× and 400× magnification were performed using a microscopic imaging system (Nikon DS-Fi2, Nikon, Japan) with an optical microscope (Nikon Eclipse Ci-L, Nikon, Japan). The scoring principles for HE staining were as follows (Wang et al., 2020): 0: Aorta structure is normal, no obvious damage; 1: The aortic structure was slightly damaged and the artery wall slightly thickened; 2: The aortic structure was slightly damaged, the artery wall was slightly thickened, and there was mild AS. 3: The aortic structure had moderate damage, the arterial wall had moderate thickening, and there was moderate AS. 4: The aortic structure was severely damaged, the artery wall was severely thickened, and there was severe AS.

Masson staining

The aorta tissue slides were baked at 62°C for 2h, de-waxed with xylene and gradient ethanol, washed with water, and stained with Weigert hematoxylin, Ponceau staining solution, phosphomolybdate liquid, and aniline blue liquid. The slides were dehydrated using gradient ethanol and sealed with neutral gum. The images of aortic fibrosis at 200× magnification were observed and pictured using the microscopic imaging system with the optical microscope.

Immunofluorescence assay (IF)

The aorta tissue slides were de-waxed and washed, and the activity of endogenous peroxidase was blocked with 3% H_2O_2. Then, slides were immersed in boiling antigen retrieval solution for 15 min and washed with PBS. 5% BSA was used to block the slides, and the CD68 antibody diluent to a 1:300 dilution was added and incubated at 4°C for 12h. The following day, a secondary antibody was added and incubated for 0.5 h at 37°C away from light, followed by incubating with try-488 tyramine conversion reagent. Afterward, the steps of antigen retrieval, blocking, incubating with LC3B antibody (1:300 dilution), and a secondary antibody, incubating with try-cy3 tyramine conversion reagent were repeated. Finally, anti-fluorescence quenching sealers (DAPI contained) were added and the images were captured by a fluorescence microscope (Ts2-FC, Nikon, Japan).

Biochemical assay

The TC and TG levels of mouse sera were detected using biochemical kits according to the instructions. The absorbance was determined using a microplate reader (CMaxPlus, MD, USA) at 510 nm.

Cell culture and grouping

RAW264.7 (mouse monocyte, iCell-m047) cells were obtained from iCell Bioscience Inc (Shanghai, China). RAW264.7 were cultured in DMEM high-glucose medium containing 10% FBS and 100 U/mL penicillin-streptomycin in a cell incubator (5% CO_2, 37°C). The medium was changed every other day.

RAW264.7 were divided into four groups: the Control group and THP groups (5, 10, 20 μg/mL THP) to detect the effect of THP on cell viability. Then, five groups were used: the Control group, ox-LDL group (50 μg/mL ox-LDL), and THP groups (50 μg/mL ox-LDL + 5, 10, 20 μg/mL THP) to determine the effects of THP on ox-LDL-incubated RAW264.7. Finally, four groups were used: the Control group, ox-LDL group (50 μg/mL ox-LDL), THP group (10 μg/mL THP), and THP + Ara-A group (10 μg/mL THP + 0.5 mM Ara-A) to verify the mechanisms of THP.

MTT assay

RAW264.7 were inoculated into 96-well plates at 1×10^4 cells/well. Different concentrations (5, 10, 20 μg/mL) of THP were added and cultured for 24h. Finally, 20 μL of MTT solution was added to each well and incubated in a cell incubator (5% CO_2, 37°C) for 4h. Afterward, the plates were centrifuged at 1,500 rpm/min for 10 min and the medium discarded. Then, 100 μL DMSO was added to each well and the plates were gently shaken for 20 min. After the purple-blue crystals were completely dissolved, the absorbance value was determined by the microplate reader at 490 nm.

Cholesterol uptake assay

25-NBD cholesterol is a fluorescent-tagged cholesterol. RAW264.7 cells were inoculated into 96-well plates and cultured for 6h. Then, serum-free DMEM containing 25-NBD cholesterol (5 μg/mL) and different concentrations of THP (5, 10, 20 μg/mL) were

added and cultured for different times (0.5h, 1h, 2h, 4h, 6h). The medium was removed and cells were washed with PBS, and the fluorescence intensity was detected immediately using the microplate reader at 485/535 nm.

Cholesterol efflux assay

Control RAW264.7 and ox-LDL-loading RAW264.7 were first treated with NBD cholesterol (5 μmol/L) for 6h. Afterward, serum-free DMEM containing HDL and different concentrations of THP (5, 10, 20 μg/mL) were added and cultured for 6h. Cell supernatant and cell lysate were collected and the fluorescence intensities were detected by the microplate reader at 485/523 nm.

ELISA

Lipid metabolism indexes LDL, HDL levels of the mice serum, and inflammatory factors MCP-1, TNF-α, and IL-6 levels of mouse sera or cell culture supernatants were determined using ELISA according to the instructions. Their levels were calculated according to standard curves.

Oil red staining

The lipid concentration in tissues or cells was usually detected using oil red staining. The aorta tissues or RAW264.7 cells were fixed in 4% paraformaldehyde and washed with water or PBS. Then, samples were washed with 60% isopropanol and soaked with oil red staining reagent. The aorta tissues were immersed in the oil red solution at 37°C for 20 min away from light, differentiated using 60% isopropanol, and stopped with water, followed by recording with the camera (850D, Canon Ltd., Japan). RAW264.7 were stained with oil red staining reagent overnight and washed with water. After air drying, the lipid concentration of cells was observed and photographed with the optical microscope. The oil red in the cells was melted with isopropanol, followed by absorbing 200 μL into the 96-well plates and the absorbance was detected using the microplate reader at 490 nm.

Transmission electron microscope (TEM)

TEM can be used to observe autophagosomes. Approximately 1 mm^3 of aorta tissues were isolated and RAW264.7 cells were collected to analyze autophagy by TEM. After fixing with 2.5% glutaraldehyde, the samples were fixed with 1% osmic acid fixative. Afterward, the samples were dehydrated in gradient ethanol. The aorta tissues were immersed in epoxy propane and embedded with pure epoxy resin followed by cutting into 70 nm slices. The slices were stained with 2% uranium acetate saturated alcohol solution and lead citrate. Autophagosomes in aorta tissues were observed using a TEM (JEM1400, JEOL Ltd., Japan). In addition, RAW264.7 cells were soaked in ethylene oxide and penetrated with a gradient acetone mixture. The cells were polymerized with epon at 70°C overnight, cut into 70 nm slices, and staining was performed as described above for aorta tissues. The autophagosomes in cells were also observed using TEM.

q-PCR

The RNA of RAW264.7 was extracted with a special kit (AG21024, Amyjet) according to the manufacturer's instructions. Real-time fluorescence qPCR was performed on a Roche LightCycler® 96 instrument following standard protocols. The amplification parameters were set as follows: denaturation at 95°C for 10 min, followed by 40 cycles at 95°C for 15 s and at 60°C for 60 s. The Primer sequences used in qPCR are listed in Table 1.

Western Blot

The total protein of frozen aorta tissues or cell samples was extracted and 10% or 12% SDS-PAGE was prepared to separate different molecular weights proteins at 80 V-120 V. Then, the proteins were transferred to the PVDF membranes at 200 mA for 2h. Immediately after, the PVDF membranes were blocked with 5% BSA for 2h at 22°C and immediately incubated with primary antibodies against AMPK, p-AMPK, mTOR, p-mTOR, P62, and LC3 at a dilution of 1:1000 and GAPDH at a dilution of 1:10000 at 4°C for 12h. Then, a secondary antibody (1:6000 dilution) was added to incubate membranes for 2h at 22°C. Ultra-ECL chemiluminescent solution was prepared and the protein images were captured using a chemiluminescence apparatus (610020-9Q, Shanghai Qinxiang Scientific Instrument Co., LTD, China). The protein bands were analyzed by Image-J.

Statistical analysis

The data analysis was performed via SPSS 20.0. The

Table 1. Primer sequence.

Gene	Forward Primer	Reverse Primer
Mouse Beclin-1	ATGGAGGGGTCTAAGGCGTC	TGGGCTGTGGTAAGTAATGGA
Mouse MCP-1	CTGAGTTGACTCCTACTGTGGA	TCTTCCCAGGGTCGATAAAGT
Mouse β-actin	GTGTGATGGTGGGAATGGGT	ACTCCTGCTTGCTGATCCAC

quantitative data were analyzed by using One-way analysis of variance (ANOVA) followed by Tukey's post-tests. If the distribution was normal but the variance was not uniform, Dunnett's T3 test was used. If data did not conform to the normal distribution, the Kruskal-Wallis H test was used. All data were expressed as mean ± standard deviation (SD) and $p<0.05$ was defined as a significant difference between groups.

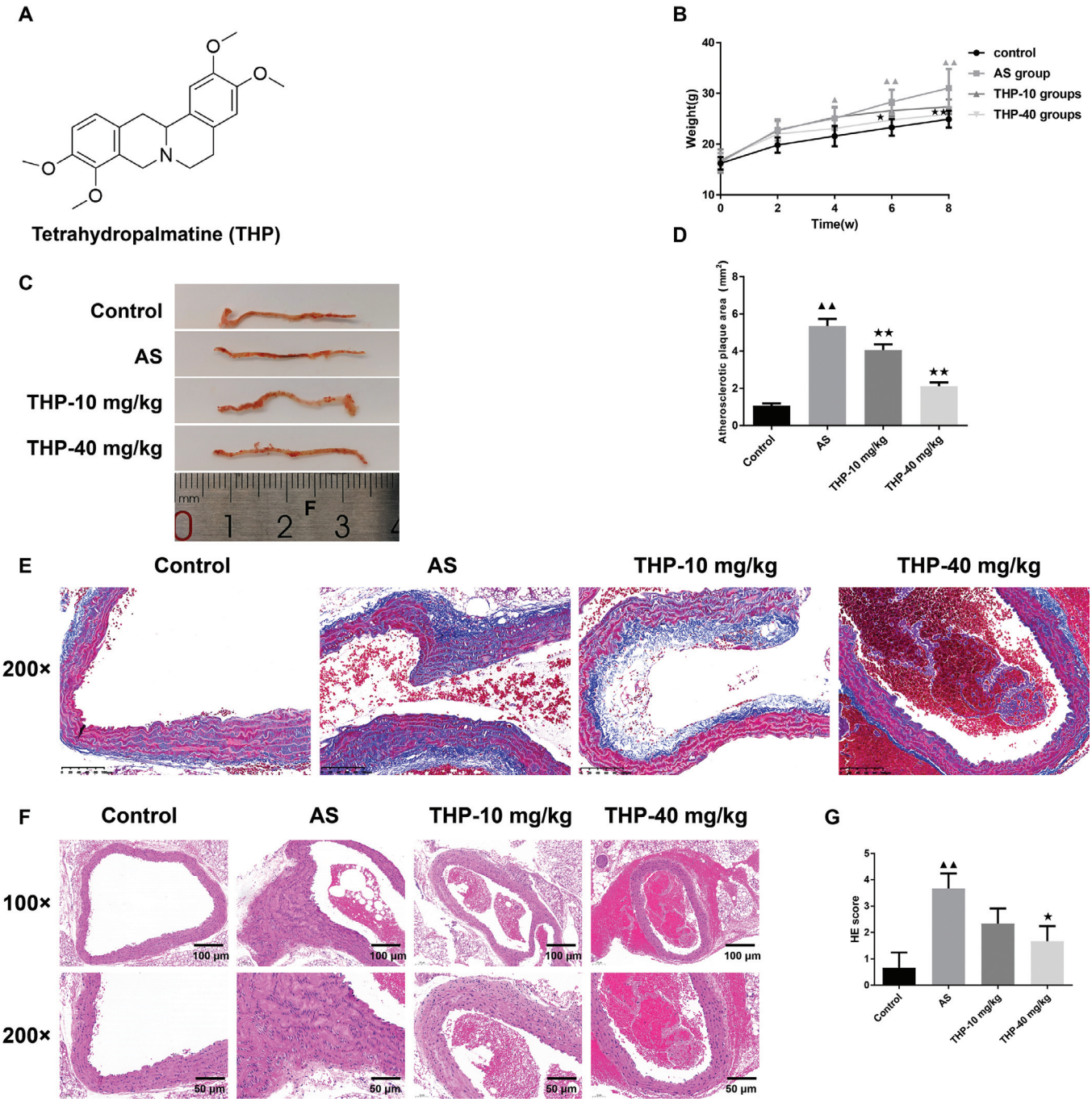

Fig. 1. Tetrahydropalmatine (THP) alleviates atherosclerosis (AS) lesions of aorta tissues in high-fat diet apolipoprotein E-deficient (ApoE$^{-/-}$) mice. ApoE$^{-/-}$ mice received a high-fat diet for 8 weeks and were treated with or without THP for 8 weeks. **A.** The chemical structure formula of THP. **B.** The mouse body weight curve. **C, D.** Representative images of oil red staining of aorta and plaque area statistics in AS mice aorta. **E.** Representative images of Masson staining of AS mice aorta. **F.** Representative images of Hematoxylin and Eosin (HE) staining. **G.** HE scores. Data are presented as the mean±SD, n=3. ▲▲$p<0.01$ vs. the Control group; ★$p<0.05$, ★★$p<0.01$ vs. the AS group. Scale bars: E, F, 100 μm

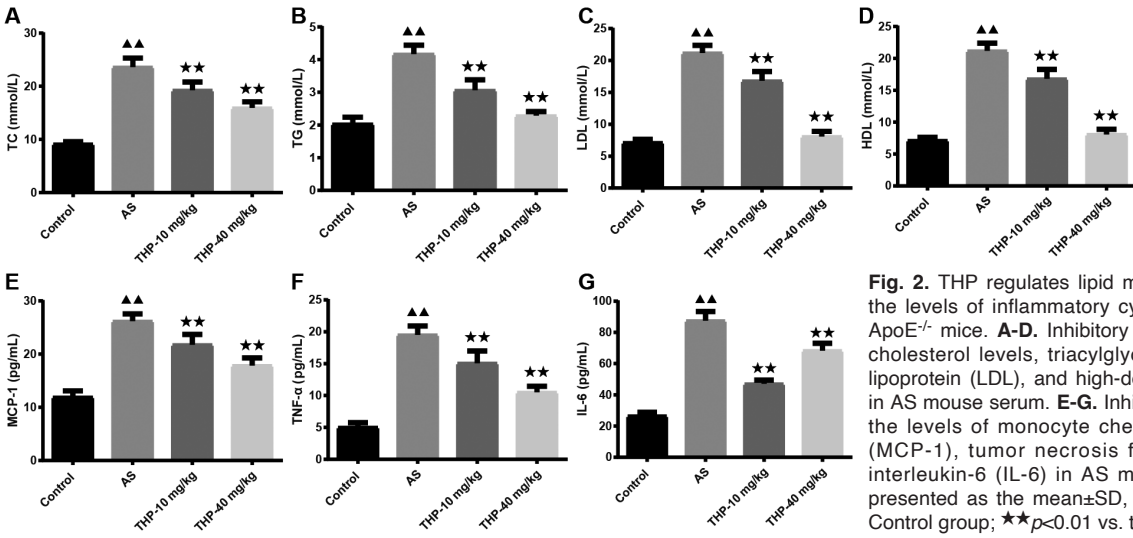

Fig. 2. THP regulates lipid metabolism and reduces the levels of inflammatory cytokines in high-fat diet ApoE$^{-/-}$ mice. **A-D.** Inhibitory effects of THP on total cholesterol levels, triacylglycerol (TG), low-density lipoprotein (LDL), and high-density lipoprotein (HDL) in AS mouse serum. **E-G.** Inhibitory effects of THP on the levels of monocyte chemoattractant protein-1 (MCP-1), tumor necrosis factor-α (TNF-α), and interleukin-6 (IL-6) in AS mouse serum. Data are presented as the mean±SD, n=6. ▲▲p<0.01 vs. the Control group; ★★p<0.01 vs. the AS group.

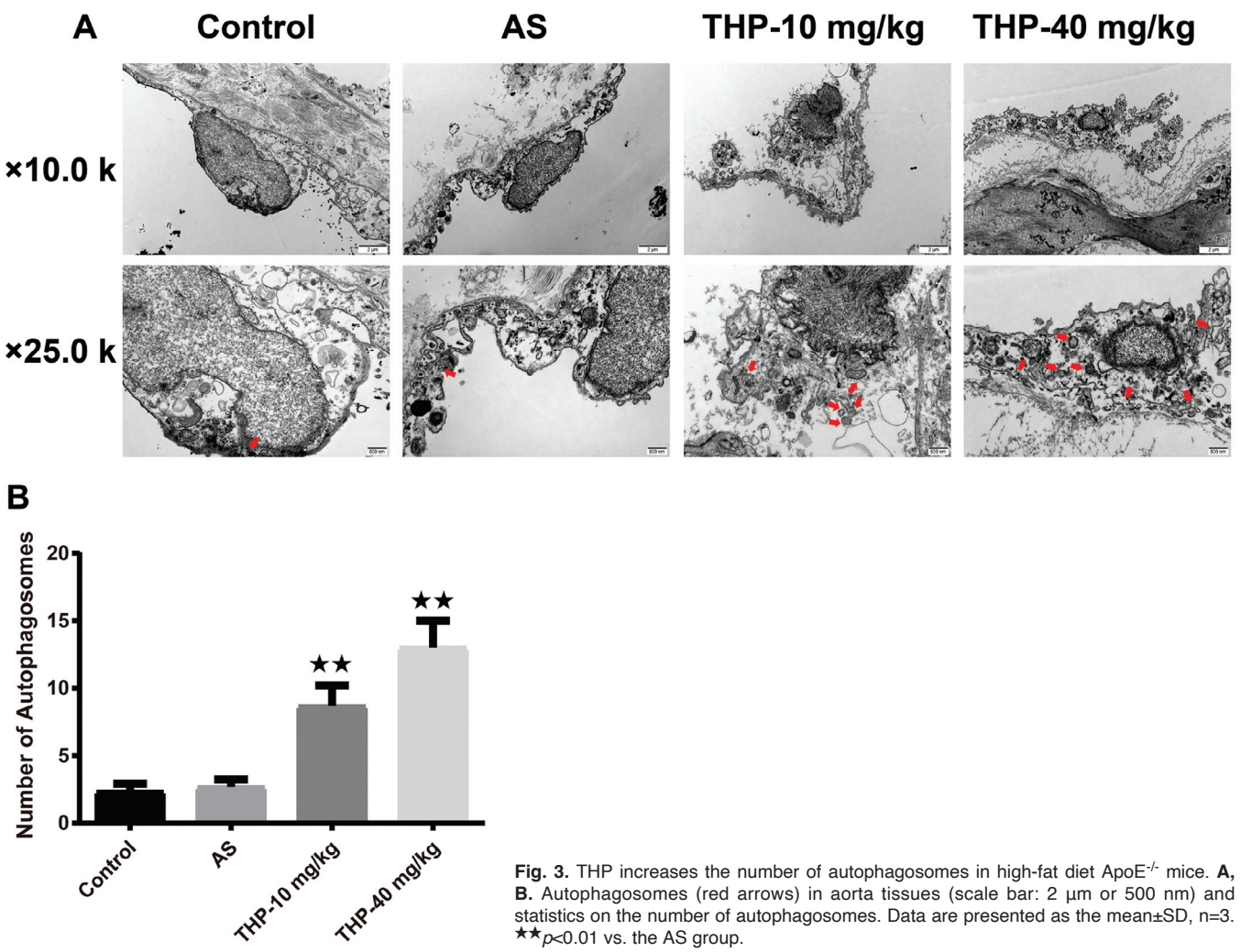

Fig. 3. THP increases the number of autophagosomes in high-fat diet ApoE$^{-/-}$ mice. **A, B.** Autophagosomes (red arrows) in aorta tissues (scale bar: 2 μm or 500 nm) and statistics on the number of autophagosomes. Data are presented as the mean±SD, n=3. ★★p<0.01 vs. the AS group.

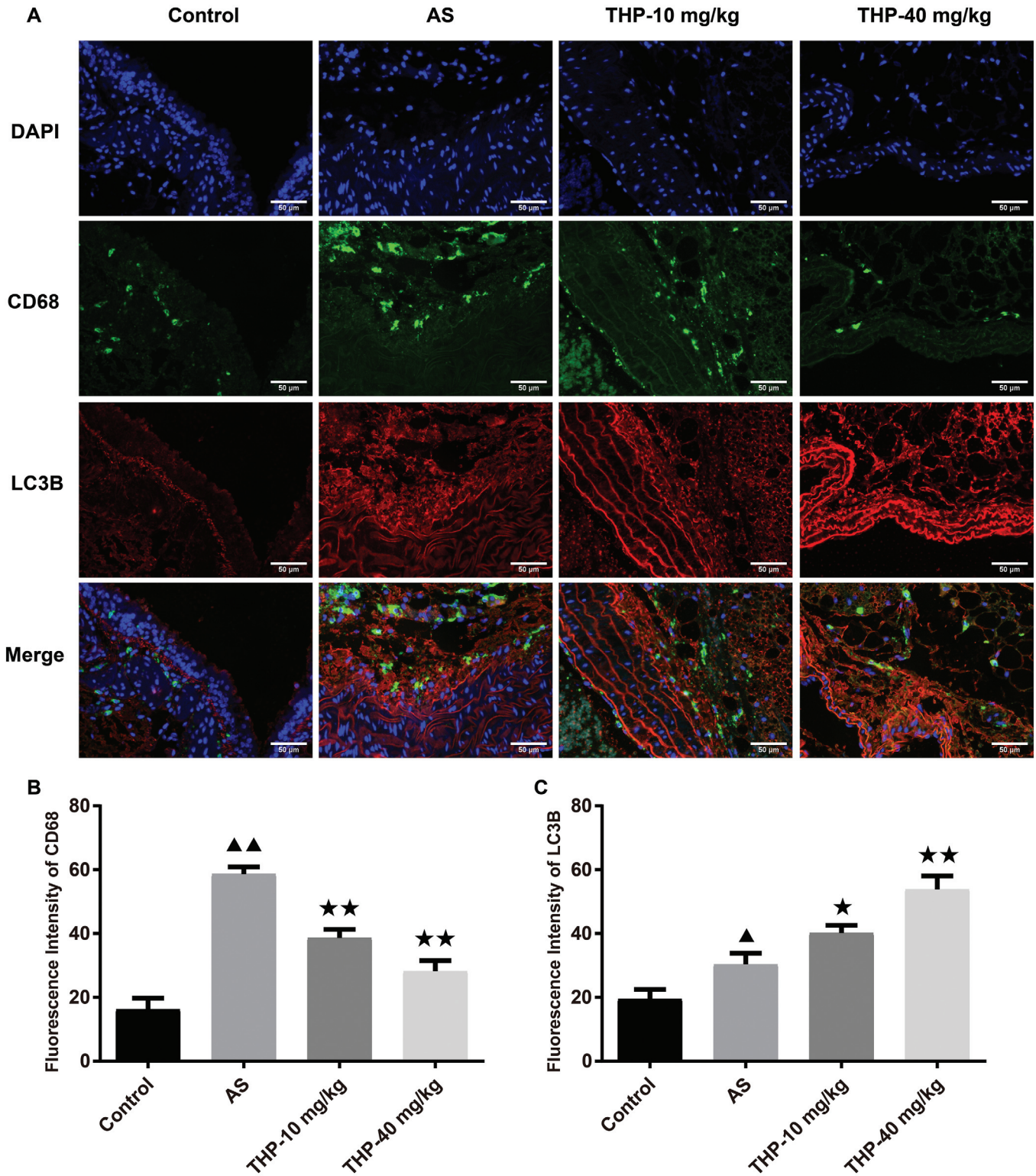

Fig. 4. THP regulates the expression of macrophage autophagy-related proteins in high-fat diet ApoE$^{-/-}$ mice. **A-C.** Representative images of aorta tissues with co-staining of CD68 (green), LC3B (red), and nuclear (blue) (scale bar: 50 μm) and corresponding quantitative statistical results. Data are presented as the mean ± SD, n=3. ▲p<0.05 vs. the Control group; ★★p<0.01 vs. the AS group.

Results

THP alleviates the AS lesions of aorta tissues in high-fat diet ApoE$^{-/-}$ mice

Figure 1A shows the chemical structure of THP. As shown in Figure 1B, compared with the control group, the body weight of AS mice increased significantly after week 4 (p<0.05 or p<0.01). Notably, after 6 weeks of 40 mg/kg THP administration, body weight in the THP40 group decreased significantly (p<0.05 or p<0.01). As shown in Figure 1C,D, after oil red O staining, a significant increase in red-stained lipid deposits around the aorta surface was observed in the AS group compared with the control group (p<0.01). In addition, only the AS group exhibited dark red plaques within the aorta, indicating severe AS damage. After THP treatment, the red-stained lipid deposits were reduced and the AS plaque area was decreased (p<0.01). The Masson staining results (Fig. 1E) showed that compared with the control group, the observed increase in the blue-stained fibrotic area, coupled with the presence of numerous cavities within the aortic tissue, indicated significant damage caused by AS. However, after THP treatment, fibrotic areas and cavities were reduced, suggesting that THP mitigated AS damage. The aortic fibrosis decreased with THP treatment. The results of HE staining (Fig. 1F,G) revealed that the aortic structure was severely damaged and the arterial wall was severely thickened in AS mice, indicating severe AS (p<0.01). With the intervention of 40 mg/kg THP, arterial wall thickening, hyperplasia, and AS were improved, and HE scores were reduced (p<0.05).

THP regulates lipid metabolism and reduces the levels of inflammatory cytokines in high-fat diet ApoE$^{-/-}$ mice

In Figure 2A-D, significant increases (p<0.01) in TC, TG, LDL, and HDL contents were found in the AS group, whereas THP reversed the augmentation (p<0.01). The results of serum inflammatory factors in mice (Fig. 2E-G) showed that MCP-1, TNF-α, and IL-6 levels were increased (p<0.01) in the AS group, and decreased (p<0.01) with THP treatment.

THP increases the number of autophagosomes in high-fat diet ApoE$^{-/-}$ mice

We observed the ultrastructure of aortic endothelial cells through TEM. As shown in Figure 3A, the red arrows point to typical autophagosomes, the vacuolar component with a bilayer membrane containing black-stained organelles. Autophagosomes were rarely observed in the control and AS group, whereas autophagosomes were increased in a dose-dependent manner after THP treatment.

THP regulates the expression of macrophage autophagy-related proteins in high-fat diet ApoE$^{-/-}$ mice

As shown in Figure 4A, the green signal represents the expression of CD68, a macrophage marker (Wang et al., 2017), thus colocalizing macrophages; whereas the

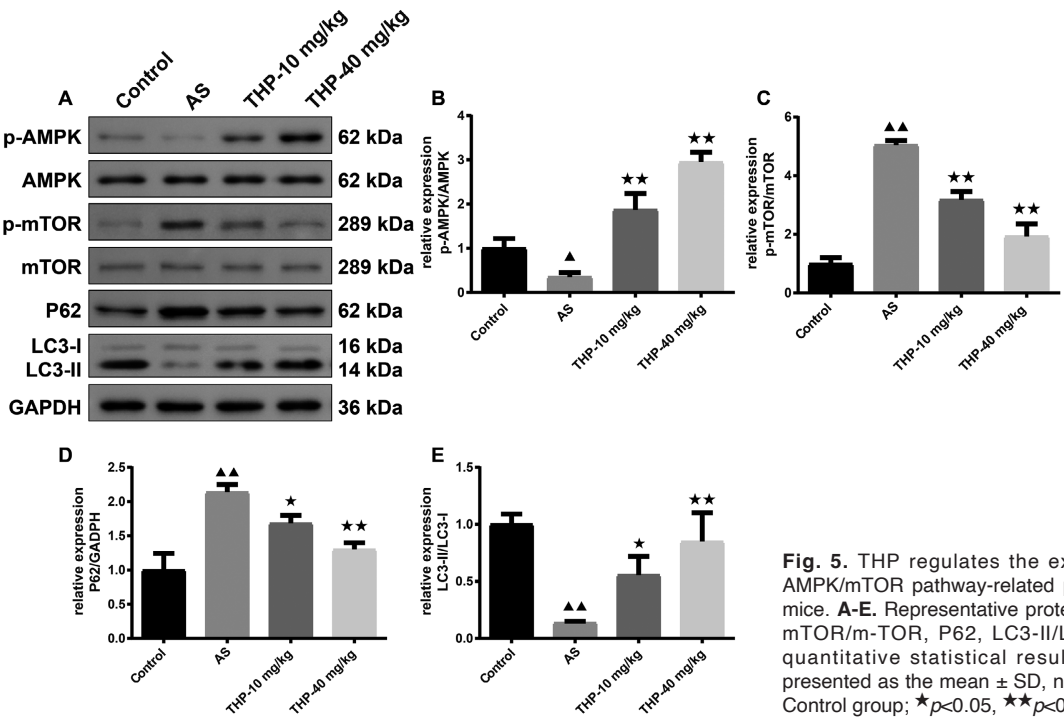

Fig. 5. THP regulates the expression of autophagy- and AMPK/mTOR pathway-related proteins in high-fat diet ApoE$^{-/-}$ mice. **A-E.** Representative protein bands of p-AMPK/AMPK, p-mTOR/m-TOR, P62, LC3-II/LC3-I and the corresponding quantitative statistical results in aorta tissue. Data are presented as the mean ± SD, n=3. ▲p<0.05, ▲▲p<0.01 vs. the Control group; ★p<0.05, ★★p<0.01 vs. the AS group.

red signal represents LC3B, serving as a widely utilized marker of autophagy (Hwang et al., 2022). The green and red signals showed a similar shape and overlapped roughly in the merged image, indicating LC3B expression in macrophages. However, IF results (Fig. 4B,C) indicated that the expression of CD68 and LC3B was increased (p<0.01) in the AS group. With the intervention of THP, compared with the AS group, CD68 was decreased (p<0.01) while LC3B expression was further increased (p<0.05 or p<0.01).

THP regulates the expression of autophagy- and AMPK/mTOR pathway-related proteins in high-fat diet ApoE$^{-/-}$ mice

Western blot results (Fig. 5A-E) indicated that the ratio of p-AMPK/AMPK and LC3-II/LC3-I was reduced to half or lower (p<0.05 or p<0.01), and the expression of p-mTOR/mTOR and P62 was increased to double or higher (p<0.01) in the AS group. After the intervention of THP, the tendencies were reversed (p<0.05 or p<0.01).

Effects of THP on cell viability, lipid concentration, cholesterol uptake, and cholesterol efflux in ox-LDL-incubated RAW264.7

MTT assay results in Figure 6A demonstrated that THP did not significantly inhibit the cell viability of RAW264.7 until the concentration exceeded 20 μg/mL. As shown in Figure 6B,C, in comparison with the control group, the lipid concentration of macrophages

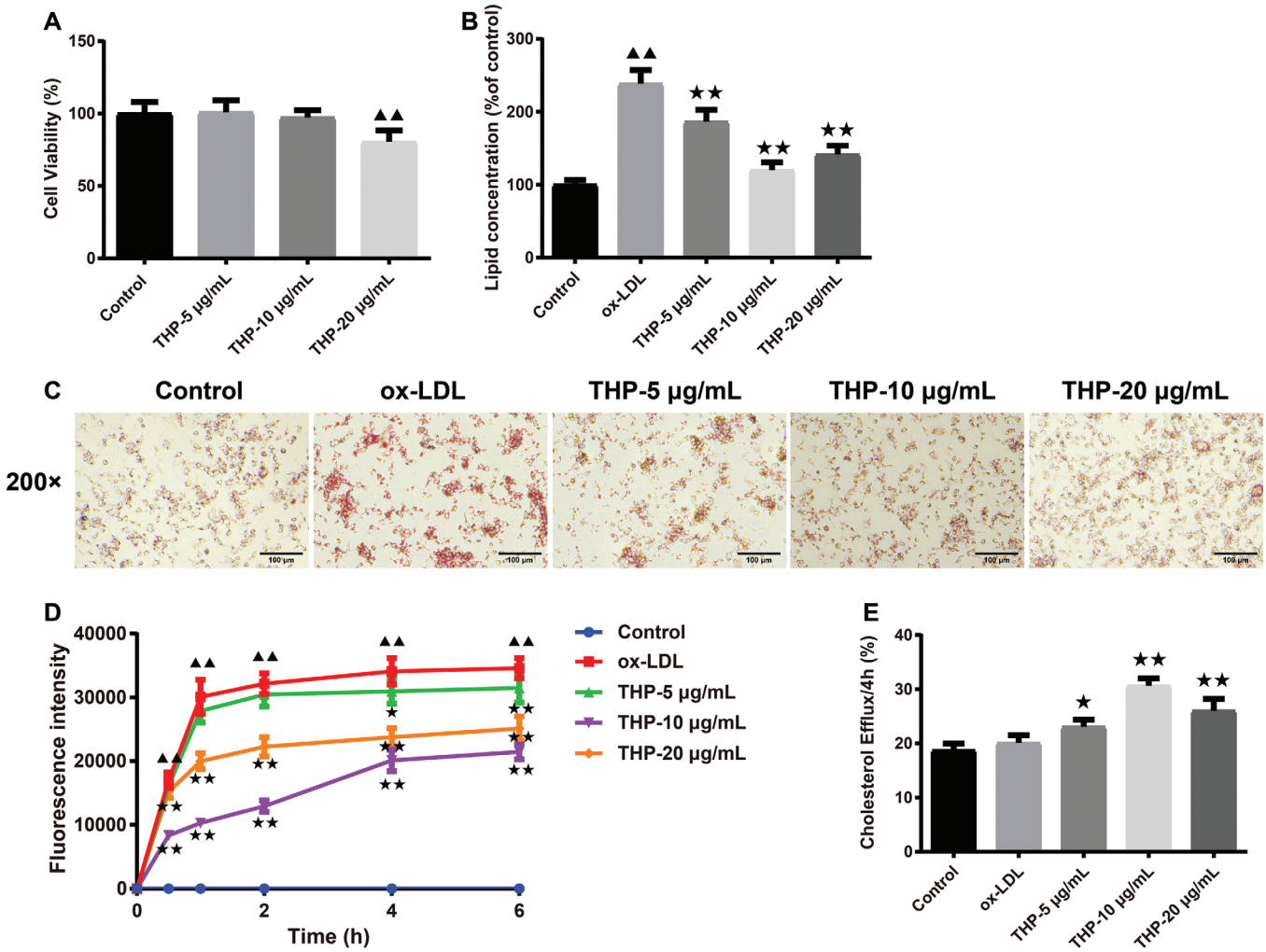

Fig. 6. Effects of THP on cell viability, lipid concentration, cholesterol uptake, and cholesterol efflux in ox-LDL-incubated RAW264.7 cells. RAW264.7 cells received ox-LDL alone or co-treated with THP for 24h. **A.** Effect of THP on the cell viability of RAW264.7 was detected by MTT (n=6). **B, C.** Effect of THP on lipid concentration in ox-LDL-incubated RAW264.7 (n=3). **D.** Inhibitory effect of THP on cholesterol uptake in ox-LDL-incubated RAW264.7 (n=6). **E.** Promotion effect of THP on cholesterol efflux in ox-LDL-incubated RAW264.7 (n=6). Data are presented as the mean ± SD. ▲▲p<0.01 vs. the Control group; ★p<0.05, ★★p<0.01 vs. the ox-LDL group. Scale bar: 100 μm.

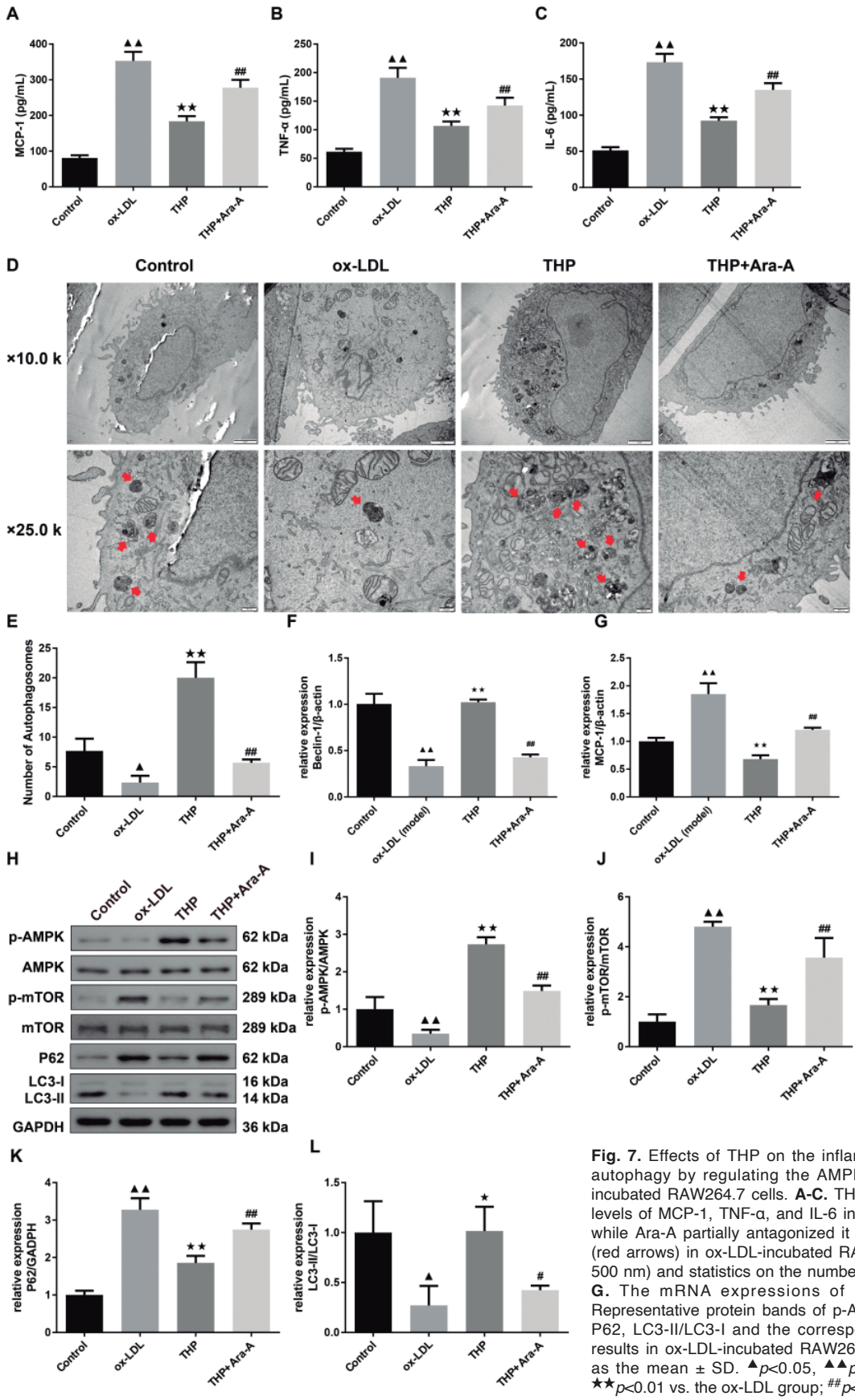

Fig. 7. Effects of THP on the inflammatory cytokines levels and autophagy by regulating the AMPK/mTOR pathway in ox-LDL-incubated RAW264.7 cells. **A-C.** THP had inhibitory effects on the levels of MCP-1, TNF-α, and IL-6 in ox-LDL-incubated RAW264.7, while Ara-A partially antagonized it (n=6). **D, E.** Autophagosomes (red arrows) in ox-LDL-incubated RAW264.7 (scale bar = 2 μm or 500 nm) and statistics on the number of autophagosomes (n=3). **F, G.** The mRNA expressions of *Beclin-1* and *MCP-1*. **H-L.** Representative protein bands of p-AMPK/AMPK, p-mTOR/m-TOR, P62, LC3-II/LC3-I and the corresponding quantitative statistical results in ox-LDL-incubated RAW264.7 (n=3). Data are presented as the mean ± SD. $^{▲}p<0.05$, $^{▲▲}p<0.01$ vs. the Control group; $^{★★}p<0.01$ vs. the ox-LDL group; $^{\#\#}p<0.01$ vs. the THP group.

increased in ox-LDL-incubated RAW264.7 ($p<0.01$), while THP decreased the lipid concentration ($p<0.01$). In Figure 6D, cholesterol uptake in the control group was almost negligible, with the other groups showing similar curves gradually plateauing, indicating a diminishing capacity for cholesterol uptake with time lag. In comparison with the ox-LDL group, the fluorescence intensity in cells of the THP-5 μg/mL group was decreased ($p<0.05$ or $p<0.01$) after 4-6h culture, whereas the THP-10 μg/mL and THP-20 μg/mL groups were significantly decreased after 0.5-6 h culture ($p<0.01$). In Figure 6E, no significant difference was observed between the control and ox-LDL groups, whereas increases in cholesterol uptake were observed after THP intervention ($p<0.05$ or $p<0.01$). Notably, we found that the cholesterol efflux rate in the THP-10 μg/mL group was higher than in the THP-20 μg/mL group, which may explain why fluorescence intensity in the THP-10 μg/mL group was lower than that of the THP-20 μg/mL group. Based on these findings, we suggested that THP suppressed cholesterol uptake and promoted cholesterol efflux in macrophages, thus reducing cholesterol accumulation.

Effects of THP on inflammatory cytokines levels and autophagy by regulating the AMPK/mTOR pathway in ox-LDL-incubated RAW264.7

Ara-A, an AMPK inhibitor, was used to verify the effects of THP on macrophage autophagy via the AMPK/mTOR pathway. In Figure 7A-C, THP reduced MCP-1, TNF-α, and IL-6 levels in ox-LDL-incubated cells ($p<0.01$), while Ara-A reversed the tendency ($p<0.01$). In Figure 7D, the red arrows point to autophagosomes, containing a characteristic multilamellar membrane and black-stained organelles. Interestingly, the number of autophagosomes was increased ($p<0.05$) after THP treatment compared with the ox-LDL group, while the number was decreased after the intervention of Ara-A ($p<0.01$) (Fig. 7E). The same pattern was observed for Beclin-1, an autophagy biomarker, whose mRNA expression decreased in the presence of ox-LDL and increased after THP treatment ($p<0.01$). However, the increase in Beclin-1 expression was reversed by Ara-A intervention ($p<0.01$). In addition, mRNA expression of MCP-1, a key chemokine that regulates macrophage migration and infiltration, was found to show a reverse trend with Beclin-1. Treatment with THP successfully reduced elevated ox-LDL-induced *MCP-1* mRNA levels, and this effect was partially counteracted by Ara-A. Western blot results (Fig. 7H-L) revealed the ratio of p-AMPK/AMPK and LC3-Ⅱ/LC3-I was increased ($p<0.05$ or $p<0.01$), and p-mTOR/mTOR and P62 was decreased ($p<0.01$) in THP group. Ara-A reversed this effect ($p<0.05$ or $p<0.01$).

Discussion

AS is a great threat to human life with high morbidity and mortality (Herrington et al., 2016). Exploring new drugs that can effectively intervene and even reverse AS is still an important mission in clinical research. ApoE$^{-/-}$ mice are often used to study the anti-atherosclerotic effects of drugs (Song et al., 2021; Dai et al., 2022), while ox-LDL is a well-known risk factor relating to the pathogenesis of AS and used to simulate AS *in vitro* (Hua et al., 2020). In this study, we confirmed that THP treatment for AS reduced lipid deposition, regulated lipid metabolism, inhibited inflammatory responses, and promoted macrophage autophagy by activation of the AMPK/mTOR pathway in high-fat diet ApoE$^{-/-}$ mice and ox-LDL-induced RAW264.7 cells.

Lipid deposition causes plaque formation and lipid metabolism plays an important role in the pathogenesis of AS (Palmeiro et al., 2012; Liu et al., 2022). THP alleviates a series of cardiovascular and cerebrovascular diseases such as AS induced by hyperlipidemia via inhibiting lipid peroxidation, endoplasmic reticulum stress, and inflammasome activation (Ding et al., 2021). Herein, we studied the effects of THP on AS in high-fat diet mice and ox-LDL-incubated RAW264.7 cells. Our experimental results indicated AS causes lipid concentration in the aorta or RAW264.7 cells and lipid metabolism disorders, as well as impacts on cholesterol uptake and cholesterol efflux capacity. Oil red staining revealed that THP treatment extremely lessened the lipid accumulation and AS plaque area while the results indicated that THP reduced the levels of lipid metabolism indexes, increased the capacity of cholesterol uptake, and decreased the capacity of cholesterol efflux. HE and Masson staining results indicated the pathological injury of aorta tissues and THP administration could significantly alleviate this pathological injury to attenuate AS. AS is an inflammatory vascular disease caused by lipid uptake (Yang and Shang, 2023), regulating inflammasome pathways and inflammatory cytokines can represent an attractive new treatment for AS (Kong et al., 2022). Our data showed that THP inhibited the inflammatory response by reducing inflammatory factor levels, including MCP-1, TNF-α, and IL-6, suggesting that THP treatment of AS is associated with anti-inflammatory effects. Particularly, MCP-1, also known as the C-C motif chemokine ligand 2(CCL2), played an essential role in monocyte migration to the vessel wall, contributing to AS development (Potashnikova et al., 2024). As Pillai. reported, endogenously produced MCP-1/CCL2 promotes the biogenic lipid-driven oxidation of LDL in macrophages, transforming macrophages into foam cells (Pillai et al., 2021). In our study, THP treatment decreased the expression of *MCP-1* mRNA; consequently, the cholesterol uptake capacity decreased after THP treatment.

As mentioned above, the formation of macrophage foam cells plays an important role in AS (Sergin and Razani., 2014). Studies have reported that macrophage autophagy can promote lipid metabolism, reduce the

formation of foam cells, remove harmful substances in macrophages, and significantly alleviate AS (Qiao et al., 2017; Luo et al., 2020).

THP can be involved in a variety of cardiovascular and cerebrovascular diseases by regulating autophagy (Yin et al., 2022a,b). Oil red staining of cells showed that THP reduces the lipid concentration to destroy the formation of foam cells in macrophages. Interestingly, increased autophagosome numbers and autophagy-related protein expression were observed in the THP groups *in vivo* and *in vitro*, suggesting the possibility of THP attenuating AS via the promotion of autophagy. *In vivo* experiments, IF results showed that LC3B expression was increased while CD68 expression was decreased in aorta tissues after THP treatment. LC3-II/LC3-I is a common standard for observing autophagy activity (Masuda et al., 2022), and the decreased ratio indicated the inhibition of autophagosome formation in AS. Beclin-1 is another biomarker of autophagy (Dai et al., 2019) and expression of Beclin-1 mRNA was observed to increase after THP treatment, indicating an enhancement in Treg autophagy. P62 is the link between LC3 and polyubiquitinated proteins (Shiozaki et al., 2020) and induction of autophagy down-regulates the expression of the P62 protein, which suggests that THP plays a promoting role in macrophage autophagy to alleviate AS.

AMPK is involved in many signal transduction pathways and is an important kinase in energy homeostasis (Herzig and Shaw, 2018). Activation of the AMPK/mTOR pathway leads to autophagy impairment (Kim et al., 2011; Mihaylova and Shaw, 2011). The animal experiment showed the effect of THP on AMPK/mTOR pathway-related proteins, the phosphorylated AMPK levels were increased and phosphorylated mTOR was decreased after THP treatment. In cell experiments, we confirmed that THP enhanced macrophage autophagy through inhibiting the AMPK/mTOR pathway by using Ara-A, which inhibits AMPK activity to achieve autophagy inhibition (Dai et al., 2019). We found that Ara-A could reverse the decrease in inflammatory factors and the increase in autophagosome number after THP treatment. In addition, THP regulated the AMPK/mTOR pathway and increased autophagy *in vivo* and *in vitro*, while Ara-A significantly reversed it. These results suggested that autophagy played an important role in the treatment of AS and THP activated the AMPK/mTOR pathway to promote macrophage autophagy.

However, there were some limitations in our study. Whether AMPK inhibitors can reverse the effects of THP *in vivo* has not been demonstrated. Thus, shRNA built on viral vectors will be used in further *in vivo* experiments. In addition, the sample size was small and we did not establish a positive control group both *in vivo* and *in vitro*, which reduced the persuasiveness of our conclusion. It is worth noting that lipid concentration, cholesterol uptake, and efflux rate assays revealed better protection with THP-10 μg/mL against macrophage lipid overload than with THP-20 μg/mL. More experiments, such as Western blot analysis for the expression of proteins related to autophagy or the AMPK/mTOR pathway, are needed to uncover the mechanism. Furthermore, the target genes of THP for macrophage autophagy are still unclear, while further metabolomics and gene sequencing are required.

Conclusions

In conclusion, in high-fat diet, ApoE$^{-/-}$ mice, aortic pathological injury, lipid metabolism disorders, inflammation, and hypoautophagy occur in AS, and THP intervention could regulate autophagy and AMPK/mTOR pathway-related proteins to promote autophagy to protect against AS. In addition, THP could inhibit ox-LDL-induced lipid concentrations and inflammation, regulate cholesterol uptake and efflux, and regulate autophagy and AMPK/mTOR pathway-related proteins to promote autophagy in RAW264.7. Our findings indicated that THP promotes macrophage autophagy by inhibiting the AMPK/mTOR pathway to attenuate AS.

Funding. This work was supported by The Seventh National Academic Experience Inheritance Project of Senior TCM Experts of the State Administration of TCM.

Conflict of interests. The authors report no conflict of interest. *Authors' contributions*. Conception and design of the research: Ke Ding. Acquisition of data: Jiaqi He. Analysis and interpretation of data: Jiaqi He. Statistical analysis: Jiahong Wang. Drafting the manuscript: Ke Ding. Revision of the manuscript for important intellectual content: Hui Wang. Approval of the final version of the manuscript to be published: All authors. Agreement to be accountable for all aspects of the work ensuring that questions related to the accuracy or integrity of the work are appropriately investigated and resolved: Ke Ding, Jiaqi He, Jiahong Wang, Hui Wang.

Ethics approval. The experimental animals were reviewed by the Experimental Animal Ethics Committee of Zhejiang Eyoung Pharmaceutical Research and Development Co., Ltd (License No.: SYXK (Zhe) 2021-0033).

Data availability statement. The data presented in this study are available upon request from the corresponding author.

References

Bai T., Li M., Liu Y., Qiao Z. and Wang Z. (2020). Inhibition of ferroptosis alleviates atherosclerosis through attenuating lipid peroxidation and endothelial dysfunction in mouse aortic endothelial cell. Free Radic. Biol. Med. 160, 92-102.

Cao H., Jia Q., Yan L., Chen C., Xing S. and Shen D. (2019). Quercetin suppresses the progression of atherosclerosis by regulating MST1-Mediated autophagy in ox-LDL-induced RAW264.7 macrophage foam cells. Int J Mol Sci, 20, 6093.

Cao Q., Du H., Fu X., Duan N., Liu C. and Li X. (2020). Artemisinin attenuated atherosclerosis in high-fat diet-fed ApoE$^{-/-}$ mice by promoting macrophage autophagy through the AMPK/mTOR/ULK1 pathway. J Cardiovasc Pharmacol, 75, 321-332.

Chistiakov D., Melnichenko A., Myasoedov, V., Grechko A.V. and

Orekhor A.N.. (2017). Mechanisms of foam cell formation in atherosclerosis. J Mol Med, 95, 1153-1165.

Dai S., Hou A., Zha S., Chen X.-M., Huang H.-T., Chen B.-H. and Kong H.-L. (2019). Ginsenoside Rb1 ameliorates autophagy of hypoxia cardiomyocytes from neonatal rats via AMP-activated protein kinase pathway. Chin. J. Integr. Med. 25, 521-528.

Dai Z., Li S., Meng Y., Zhao Q., Zhang Y., Suonan Z., Sun Y., Shen Q., Liao X and Xue Y. (2022). Capsaicin ameliorates high-fat diet-induced atherosclerosis in ApoE$^{-/-}$ mice via remodeling gut microbiota. Nutrients 14, 4334-4347.

Ding K., Chen L., He J., Wang J., Yu C. and Wang H. (2021). Tetrahydropalmatine alleviates hyperlipidemia by regulating lipid Peroxidation, endoplasmic retiulum Stress, and inflammasome activation by inhibiting the TLR4-NF-κB Pathway. Evid. Based Complement. Alternat. Med. 2021, 6614985.

Emanuel R., Sergin I., Bhattacharya S., Turner J., Epelman S., Settembre C., Diwan A., Ballabio A. and Razani B. (2014). Induction of lysosomal biogenesis in atherosclerotic macrophages can rescue lipid-induced lysosomal dysfunction and downstream sequelae. Arterioscler. Thromb. Vasc. Biol. 34, 1942-1952.

Evans T., Jeong S., Zhang X., Sergin I. and Razani B. (2018). TFEB and trehalose drive the macrophage autophagy-lysosome system to protect against atherosclerosis. Autophagy 14, 724-726.

Fan X., Wang J., Hou J., Lin C., Bensoussan A., Chang D., Liu J. and Wang B. (2015). Berberine alleviates ox-LDL induced inflammatory factors by up-regulation of autophagy via AMPK/mTOR signaling pathway. J. Transl. Med. 13, 92.

Guan F., Yu B., Qi G., Hu J., Zeng D.-Y. and Luo J. (2008). Chemical hypoxia-induced glucose transporter-4 translocation in neonatal rat cardiomyocytes. Arch. Med. Res. 39, 52-60.

Herrington W., Lacey B., Sherliker P., Armitage J. and Lewington S. (2016). Epidemiology of atherosclerosis and the potential to reduce the global burden of atherothrombotic disease. Circ. Res. 118, 535-546.

Herzig S. and Shaw R. (2018). AMPK: guardian of metabolism and mitochondrial homeostasis. Nat. Rev. Mol. Cell Biol. 19, 121-135.

Hua Z., Ma K., Liu S., Yue Y., Cao H. and Li Z. (2020). LncRNA ZEB1-AS1 facilitates ox-LDL-induced damage of HCtAEC cells and the oxidative stress and inflammatory events of THP-1 cells via miR-942/HMGB1 signaling. Life Sci. 247, 117334.

Hwang H., Ha H., Lee B., Kim B.H., Song H.K. and Kim Y.K. (2022). LC3B is an RNA-binding protein to trigger rapid mRNA degradation during autophagy. Nat. Commun. 13, 1436.

Kim J., Kundu M., Viollet B. and Guan K.-L. (2011). AMPK and mTOR regulate autophagy through direct phosphorylation of Ulk1. Nat. Cell Biol. 13, 132-141.

Kong P., Cui Z., Huang X., Zhang D.-D., Guo R.-J. and Han M. (2022). Inflammation and atherosclerosis: Signaling pathways and therapeutic intervention. Signal Transduct. Target Ther. 7, 131.

Liang S., Hu J., Zhang A., Li F. and Li X. (2020). *miR-155* induces endothelial cell apoptosis and inflammatory response in atherosclerosis by regulating Bmal1. Exp. Ther. Med. 20, 128.

Liu W., Östberg N., Yalcinkaya M., Dou H., Endo-Umeda K., Tang Y., Hou X., Xiao T., Fidler T.P., Abramowicz S., Yang Y.-G., Soehnlein O., Tall A.R. and Wang N. (2022). Erythroid lineage Jak2V617F expression promotes atherosclerosis through erythrophagocytosis and macrophage ferroptosis. J. Clin. Invest. 132, e155724.

Luo Y., Lu S., Gao Y., Yang K., Wu D., Xu X., Sun G. and Sun X. (2020). Araloside C attenuates atherosclerosis by modulating macrophage polarization via Sirt1-mediated autophagy. Aging (Albany NY), 12, 1704-1724.

Mao X., Pan C., Huang P., Huang P., Liu Y.-Y., Wang C.-S., Yan L., Hu B.-H., Chang X., He K., Mu H.-N., Li Q., Sun K., Fan J.-Y. and Han J.-Y. (2015). Levo-tetrahydropalmatine attenuates mouse blood-brain barrier injury induced by focal cerebral ischemia and reperfusion: Involvement of Src kinase. Sci. Rep. 5, 11155.

Masuda M., Yoshida-Shimizu R., Mori Y., Ohnishi K., Adachi Y., Sakai M., Kabutoya S., Ohminami H., Yamanaka-Okumura H., Yamamoto H., Miyazaki M. and Taketani Y. (2022). Sulforaphane induces lipophagy through the activation of AMPK-mTOR-ULK1 pathway signaling in adipocytes. J. Nutr. Biochem. 106, 109017.

Mihaylova M. and Shaw R. (2011). The AMPK signalling pathway coordinates cell growth, autophagy and metabolism. Nat. Cell Biol. 13, 1016-1023.

Mozaffarian D., Benjamin E., Go A., Arnett D.K., Blaha M.J., Cushman M., de Ferranti S., Després J.-P., Fullerton H.J., Howard V.J., Huffman M.D., Judd S.E., Kissela B.M., Lackland D.T., Lichtman J.H., Lisabeth L.D., Liu S., Mackey R.H., Matchar D.B., McGuire D.K., Mohler 3rd E.R., Moy C.S., Muntner P., Mussolino M.E., Nasir K., Neumar R.W., Nichol G., Palaniappan L., Pandey D.K., Reeves M.J., Rodriguez C.J., Sorlie P.D., Stein J., Towfighi A., Turan T.N., Virani S.S., Willey J.Z., Woo D., Yeh R.W., Turner M.B. and American Heart Association Statistics Committee and Stroke Statistics Subcommitte. (2015). Heart disease and stroke statistics--2015 update: a report from the American Heart Association. Circulation, 131, e29-322.

Osonoi Y., Mita T., Azuma K., Nakajima K., Masuyama A., Goto H., Nishida Y., Miyatsuka T., Fujitani Y., Koike M., Mitsumata M. and Watada H. (2018). Defective autophagy in vascular smooth muscle cells enhances cell death and atherosclerosis. Autophagy 14, 1991-2006.

Palmeiro C., Anand R., Dardi I., Balasubramaniyam N., Schwarcz M.D. and Weiss I.A. (2012). Growth hormone and the cardiovascular system. Cardiol. Rev. 20, 197-207.

Pillai S., Borah A., Le M., Kawano H., Hasegawa K. and Kumar D.S. (2021). Co-delivery of curcumin and bioperine via PLGA nanoparticles to prevent atherosclerotic foam cell formation. Pharmaceutics, 13, 1420.

Potashnikova D., Maryukhnich E., Vorobyeva D., Rusakovich G., Komissarov A., Tvorogova A., Gontarenko V. and Vasilieva E. (2024). Cytokine profiling of plasma and atherosclerotic plaques in patients undergoing carotid endarterectomy. Int. J. Mol. Sci. 25, 1030.

Qiao L., Zhang X., Liu M., Liu X., Dong M., Cheng J., Zhang X., Zhai C., Song Y., Lu H. and Chen W. (2017). Ginsenoside Rb1 enhances atherosclerotic plaque stability by improving autophagy and lipid metabolism in macrophage foam cells. Front. Pharmacol. 8, 727.

Razani B., Feng C., Coleman T., Emanuel R., Wen H., Hwang S., Ting J.P., Virgin H.W., Kastan M.B. and Semenkovich C.F. (2012). Autophagy links inflammasomes to atherosclerotic progression. Cell Metab. 15, 534-544.

Sergin I. and Razani B. (2014). Self-eating in the plaque: what macrophage autophagy reveals about atherosclerosis. Trends Endocrinol. Metab. 25, 225-234.

Shiozaki Y., Miyazaki-Anzai S., Okamura K., Keenan A.L., Masuda M. and Miyazaki M. (2020). GPAT4-generated saturated LPAs induce lipotoxicity through inhibition of autophagy by abnormal formation of

omegasomes. iScience 23, 101105.

Song P., Fang Z., Wang H., Cai Y., Rahimi K., Zhu Y., Fowkes F.G.R., Fowkes F.J.I. and Rudan I. (2020). Global and regional prevalence, burden, and risk factors for carotid atherosclerosis: a systematic review, meta-analysis, and modelling study. Lancet Glob. Health 8, e721-e729.

Song T., Wang P., Li C., Jia L., Liang Q., Cao Y., Dong P., Shi H. and Jiang M. (2021). Salidroside simultaneously reduces de novo lipogenesis and cholesterol biosynthesis to attenuate atherosclerosis in mice. Biomed. Pharmacother. 134, 111137.

Sundararajan S., Jayachandran I., Balasubramanyam M., Mohan V., Venkatesan B. and Manickam N. (2019). Sestrin2 regulates monocyte activation through AMPK-mTOR nexus under high-glucose and dyslipidemic conditions. J. Cell. Biochem. 120, 8201-8213.

Tabares-Guevara J., Villa-Pulgarin J. and Hernandez J. (2021). Atherosclerosis: immunopathogenesis and strategies for immunotherapy. Immunotherapy 13, 1231-1244.

Takeda-Watanabe A., Kitada M., Kanasaki K. and Koya D. (2012). SIRT1 inactivation induces inflammation through the dysregulation of autophagy in human THP-1 cells. Biochem. Biophys. Res. Commun. 427, 191-196.

Wang Y.-Y., Jiang H., Pan J., Huang X.-R., Wang Y.-C., Huang H.-F., To K.-F., Nikolic-Paterson D.J., Lan H.-Y. and Chen J.-H. (2017). Macrophage-to-Myofibroblast Transition Contributes to Interstitial Fibrosis in Chronic Renal Allograft Injury. J. Am. Soc. Nephrol. 28, 2053-2067.

Wang M., Li J., Cai J., Cheng L., Wang X. and Xu P. (2020). Overexpression of MicroRNA-16 alleviates atherosclerosis by inhibition of inflammatory pathways. Biomed. Res. Int. 2020, 8504238.

Wang B., Tang X., Yao L., Wang Y., Chen Z., Li M., Wu N., Wu D., Dai X., Jiang H. and Ai D. (2022). Disruption of USP9X in macrophages promotes foam cell formation and atherosclerosis. J. Clin. Invest. 132, e154217.

Wen H., Lu D., Chen H., Zhu Y., Xie Q., Zhang Z. and Wu Z. (2022). Tetrahydropalmatine induces the polarization of M1 macrophages to M2 to relieve limb ischemia-reperfusion-induced lung injury via inhibiting the TLR4/NF-κB/NLRP3 signaling pathway. Drug Dev. Res. 83, 1362-1372.

Yang X. and Shang D. (2023). The role of peroxisome proliferator-activated receptor γ in lipid metabolism and inflammation in atherosclerosis. Cell Biol. Int. 47, 1469-1487.

Yang Y., Li X., Peng L., An L., Sun N., Hu X., Zhou P., Xu Y., Li P. and Chen J. (2018). Tanshindiol C inhibits oxidized low-density lipoprotein induced macrophage foam cell formation via a peroxiredoxin 1 dependent pathway. Biochim. Biophys. Acta Mol. Basis Dis. 1864, 882-890.

Yin X., Li W., Zhang J., Zhao W., Cai H., Zhang C. Liu Z., Guo Y. and Wang J. (2021). AMPK-mediated metabolic switching is high effective for phytochemical levo-Tetrahydropalmatine (l-THP) to reduce hepatocellular carcinoma tumor growth. Metabolites, 11, 811.

Yin X., Liu Z. and Wang J. (2022a). Levo-tetrahydropalmatine promotes apoptosis of human hepatocellular carcinoma through switching energy metabolism phenotype via upregulation of mitochondrial reactive oxygen species. Zhongguo Zhong Yao Zhi 47, 6494-6504. (article in Chinese)

Yin X., Zhang J., Zhao W., Liu Z. and Wang J. (2022b). Combined Levo-tetrahydropalmatine and diphenyleneiodonium chloride enhances antitumor activity in hepatocellular carcinoma. Pharmacol. Res. 179, 106219.

Yuan Y., Li P. and Ye J. (2012). Lipid homeostasis and the formation of macrophage-derived foam cells in atherosclerosis. Protein Cell 3, 173-181.

Accepted September 6, 2024